Chapter 1

Introduction

1.1 Light and Optical field

Optical fields have a statistical nature. These optical fields may fluctuate erratically in time and space. The property of optical fields firmly confined either on the time axis or on the optical frequency axis, has been widely used in recent years. Using Maxwell's equations, the propagation of light field can be described by wave equations. In a vacuum, the wave equation is,

$$\nabla^2 \mathbf{U} - \frac{1}{c^2}\frac{\partial^2 \mathbf{U}}{\partial t^2} = 0 \tag{1.1}$$

where U is the light field, and c is the velocity of light. ∇^2 is the Laplace operator. A monochromatic solution to the equation can be given as,

$$U(r,t) = a(r)\exp(-i\omega t) \tag{1.2}$$

where $\omega = kc$ is the angular frequency, with k being the wave number defined as $k = 2\pi/\lambda$ for wavelength of light λ. $a(r)$ is the amplitude with position "r", and t represents time.

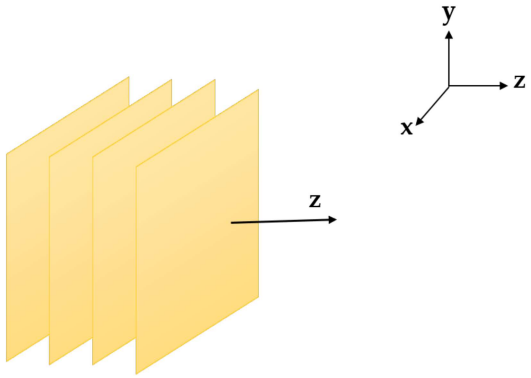

Fig. 1.1 Representation of a plane wave

Using Eq. 1.2 in Eq. 1.1 leads to the Helmholtz equation as,

$$\nabla^2 U + k^2 U = 0 \tag{1.3}$$

A solution to the Helmholtz equation in a homogeneous medium is a plane wave or spherical wave.

$$U(r) = A\exp(ik.r) \tag{1.4}$$

where A is complex amplitude.

$$U(r) = A\frac{\exp(ik.r)}{r} \tag{1.5}$$

Equations (1.4 and 1.5) describe the solutions of the Helmholtz equation for plane waves and spherical waves, respectively. Fig. 1.1 represents a plane wave. The physical importance of these solutions is that a point source produces spherical waves, which may be approximated as plane waves in the far field. Fig. 1.2 and Fig. 1.3 represents the wavefronts of plane and spherical waves respectively,Recently some interests have emerged in another unique type of wavefront, referred to as helical wavefront. A helical

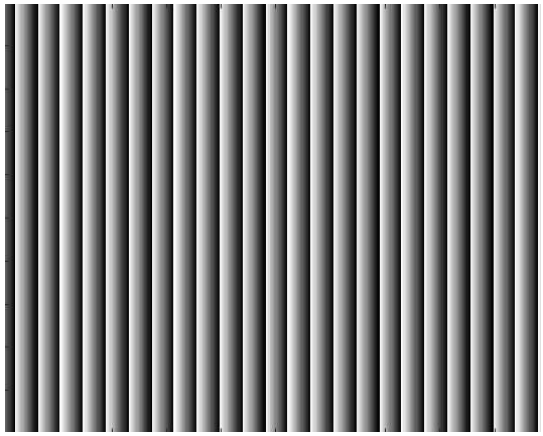

Fig. 1.2 Wavefront of plane wave

mode of light is identified by a phase factor $exp(il\phi)$, where ϕ is the azimuthal angle and l represents the topological charge[1]. In the paraxial approximation, a helical beam focuses on a dark spot; as a result, its intensity is then redistributed to a ring of light. Additionally, in contrast to their intrinsic spin angular momentum, the photons in helical beams carry a conserved orbital angular momentum [2]. A helical beam is a helical structure of a constant

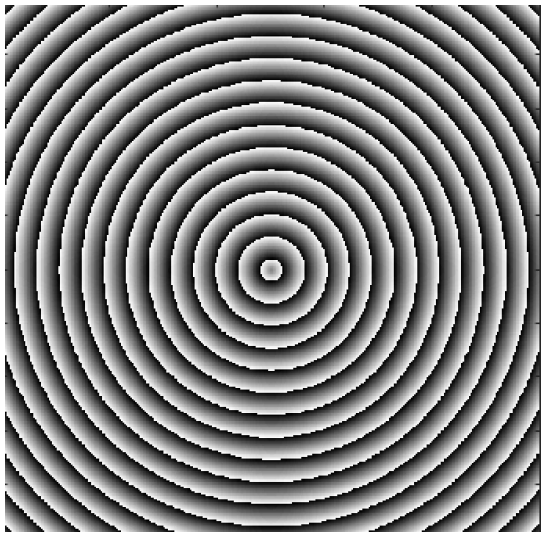

Fig. 1.3 Wavefront of spherical wave

phase surface with an indeterminate phase and zero amplitude point in its center, and this kind of beam is referred to as a "vortex beam," and this point is known as a "singular

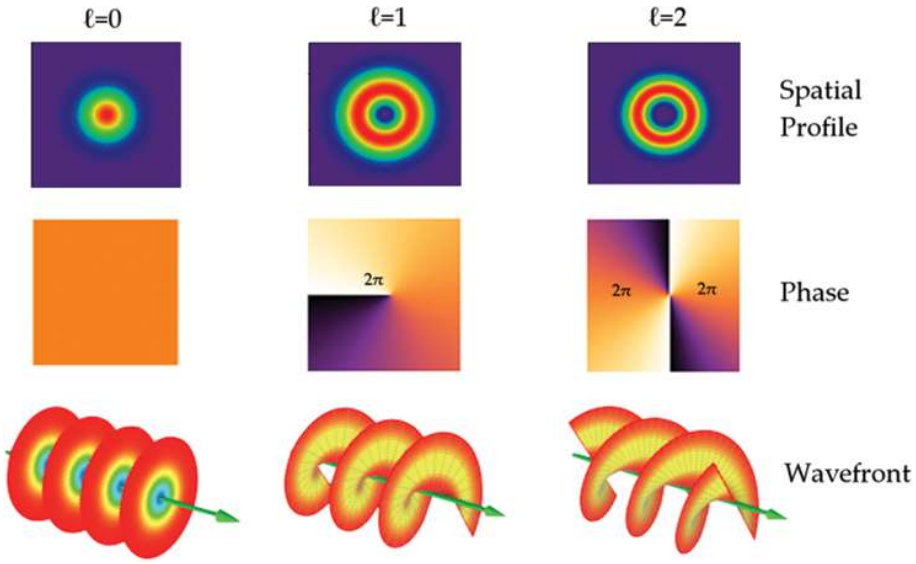

Fig. 1.4 Vortex beams representing spatial and wavefront profile with different topological charges,l=0,1,2 [3]

point." A representation of the vortex beam is shown in Fig. 1.4 [3]. Details of such waves can be found in references [4, 5, 6] in terms of imaging, diffraction, OAM holography, and information processing. Propagation of these light beams or waves through any media or free space, a natural phenomenon called ***Diffraction*** occurs to happen whenever light bends around the corner of any obstacle.

1.2 Diffraction

Diffraction is crucial in branches of science and technology where the propagation of waves is considered for different reasons. Diffraction is the key to understand the propagation of light waves through apertures and/or optical elements. Geometric optics says that when a light wave hits an obstacle, it might not act the way you would expect it to. Instead of a simple shadow on the screen behind the obstacle, a closer look shows a complicated pattern of dark and light areas. This complicated pattern, termed "diffraction," arises due to the fundamental nature of wave diffraction and superposition, and it happens when the

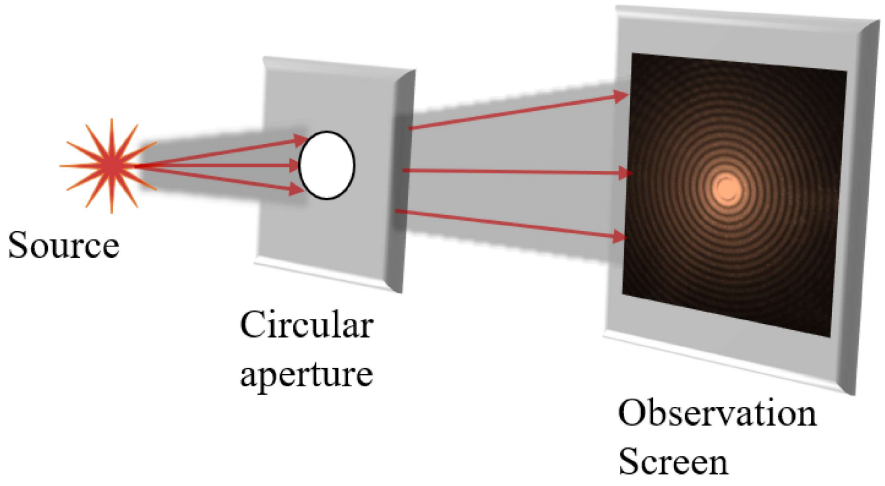

Fig. 1.5 Diffraction through far field

size of the obstruction or opening is on the same scale as the wavelength of the light. A picture of how the light gets diffracted when it passes through a circular aperture is shown in Fig. 1.5. The pattern formed at the observation plane is known as the "airy pattern," where the central part is an airy disk.

To understand diffraction more precisely, a theory was developed using Huygens's principle. Huygens, in 1678, expressed the intuitive belief that if each point on the wavefront of a disturbance was considered to be a new source of a "secondary" spherical disturbance, then the wavefront at a later instant could be determined by constructing the "envelope" of the secondary wavelets, as depicted in Fig 1.6.

1.3 Fresnel and Fraunhofer integrals

In this section, the focus is currently on a few approximations to the general theory, which will enable diffraction pattern calculations to some straightforward mathematical manipulations. Two approximations that deal with wave propagation are discussed. For a diffraction geometry given in Fig. 1.7, we will calculate the optical field at the observation

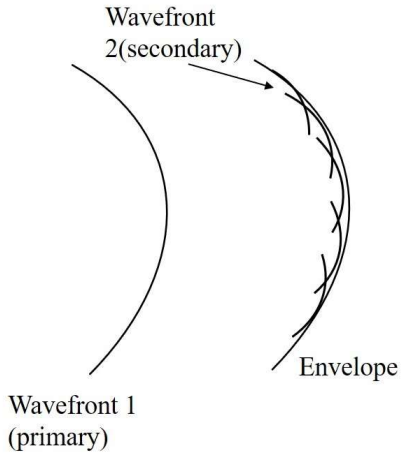

Fig. 1.6 Huygens principle

screen at a normal distance of z from the aperture plane. θ is the angle between the outward normal and a vector pointing from P to Q. From Huygens principle, the optical wavefield at the observation plane is given by,

$$E(x,y) = \frac{z}{i\lambda} \iint_{\Gamma} E(\xi,\eta) \frac{\exp(ikr_{01})}{r_{01}^2} d\xi d\eta \tag{1.6}$$

where

$$r_{01} = \sqrt{z^2 + (x-\xi)^2 + (y-\eta)^2} \tag{1.7}$$

(ξ,η) are spatial coordinates at the source plane. Now if the distance r_{01} is expanded as a binomial expansion, it leads the equation to the Fresnel approximation. Under binomial expansion,distance r_{01} can be written as,

$$r_{01} = z\sqrt{1 + \left(\frac{x-\xi}{z}\right)^2 + \left(\frac{y-\eta}{z}\right)^2}. \tag{1.8}$$

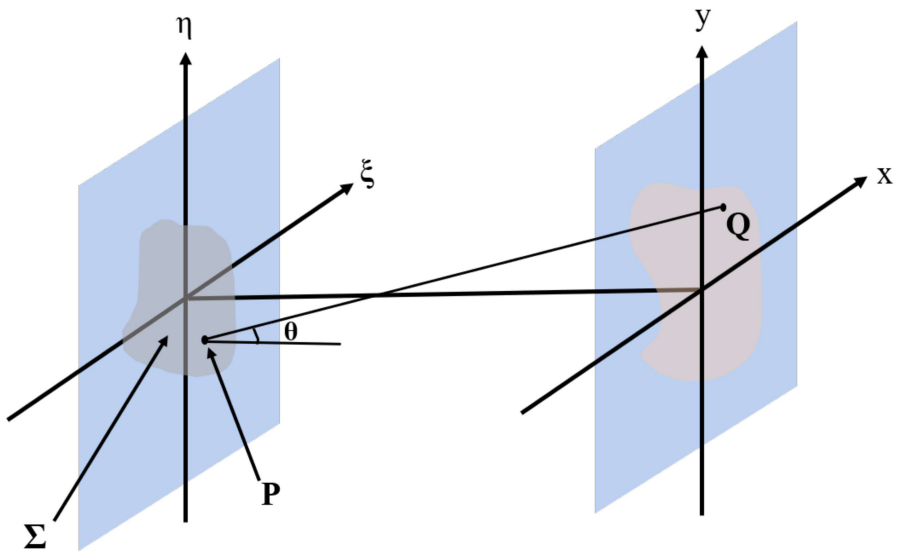

Fig. 1.7 Diffraction from aperture plane

Under the expansion condition,

$$r_{01} \approx z\left[1+\frac{1}{2}\left(\frac{x-\xi}{z}\right)^2+\frac{1}{2}\left(\frac{y-\eta}{z}\right)^2\right] \tag{1.9}$$

Using values from Eq. 1.9 in 1.6, optical wave field can be given as,

$$E(x,y)=\frac{\exp(ikz)}{i\lambda z}\iint_{-\infty}^{\infty}E(\xi,\eta)\exp\left[\frac{ik}{2z}\left((x-\xi)^2+(y-\eta)^2\right)\right]\mathrm{d}\xi\mathrm{d}\eta \tag{1.10}$$

Above equation can be written as a form of convolution given by,

$$E(x,y)=\iint_{-\infty}^{\infty}E(\xi,\eta)h(x-\xi,y-\eta)]\mathrm{d}\xi\mathrm{d}\eta \tag{1.11}$$

where $h(x-\xi,y-\eta)$ represents the kernel. Equation 1.10 represents the final form of the Fresnel diffraction integral. Equation 1.10 can be written as a two-dimensional Fourier

transform of the complex field multiplied with a phase factor, given as follows,

$$E(x,y) = \frac{\exp(ikz)}{i\lambda z}\exp(i\frac{k}{2z}(x^2+y^2))\iint_{-\infty}^{\infty} E(\xi,\eta)\exp\left[\frac{ik}{2z}\left(\xi^2+\eta^2\right)\right] \exp\left[\frac{-i2\pi}{\lambda z}\left(x\xi+y\eta\right)\right]\mathrm{d}\xi\,\mathrm{d}\eta \tag{1.12}$$

For Fraunhofer approximation, if

$$z >> \frac{k(\xi^2+\eta^2)}{2} \tag{1.13}$$

is satisfied, Eq. 1.12 can be written as,

$$E(x,y) = \frac{\exp(ikz)\exp(i\frac{k}{2z}(x^2+y^2))}{i\lambda z}\iint_{-\infty}^{\infty} E(\xi,\eta)\exp\left[\frac{-i2\pi}{\lambda z}\left(\xi x+\eta y\right)\right]\mathrm{d}\xi\,\mathrm{d}\eta \tag{1.14}$$

where $E(x,y)$ is the observed field in the far field region, i.e., Fraunhofer diffraction region.

1.3.1 Discrete Fourier transform

A two-dimensional Fourier transform of an object $t(x,y)$ is obtained at the back focal plane of the lens and is represented as [7],

$$F(f_X,f_Y) = \iint_{-\infty}^{\infty} t(x,y)\exp\left[-i2\pi\left(f_X x+f_Y y\right)\right]\mathrm{dxdy} \tag{1.15}$$

where x,y are spatial coordinates of a point in a two-dimensional space. (f_X,f_Y) represents spatial frequencies in the x and y directions and are given by, $f_X = \frac{x}{\lambda z}$, $f_Y = \frac{y}{\lambda z}$ with wavelength λ,and for focal length f, $z = f$. For the case of discrete sampling, input and output signals are represented as $x = m\Delta x$,$y = n\Delta y$ and $f_x = m^{'}\Delta f_x$,$f_y = n^{'}\Delta f_y$ respectively, where m, n and $m^{'}$, $n^{'}$ correspond to pixel numbers at input and output plane respectively.

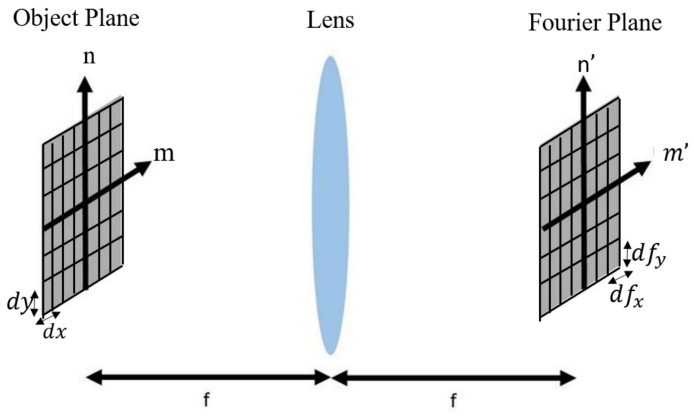

Fig. 1.8 Fourier transform with a lens

dx and dy are the pixel sizes at the input plane. Figure 1.8 represents a Fourier geometry to obtain Fourier transform using a lens focal length f. Thus a two-dimensional discrete Fourier transform (DFT) is defined as

$$F_{m',n'} = \sum_{m,n=-N/2}^{N/2-1} t_{m,n} \exp(-i\frac{2\pi}{N}(mm' + nn')) \tag{1.16}$$

where N is the length of input and output vectors.

1.3.2 Angular spectrum method

Angular spectrum is another general approach to examine and evaluate the propagation of a complex wave at any arbitrary distance from the source plane ($z = 0$). Consider a wave incident on a transverse plane traveling in the positive z direction. $E(x,y,0)$ is the complex field at plane z =0. A two-dimensional Fourier transform at plane z=0 is given by [7],

$$F(f_X, f_Y; 0) = \iint_{-\infty}^{\infty} E(x,y,0) \exp[-i2\pi(f_X x + f_Y y)] \,\mathrm{dxdy} \tag{1.17}$$

Consider a plane wave defined by $P(x,y,z)$=$exp(i\vec{k}.\vec{r})$, where the k vector is given as,

$$k = 2\pi/\lambda\,(\alpha x + \beta y + \gamma z) \tag{1.18}$$

$\vec{r}$ is a position vector and the direct cosines (α,β,γ) are related by following relation,

$$\gamma = \sqrt{1-\alpha^2-\beta^2} \tag{1.19}$$

Complex exponential function $\exp[-i2\pi\,(f_X x + f_Y y)]$ across z=0 plane may be considered as propagating with direction cosines,

$$\alpha = \lambda f_X, \beta = \lambda f_Y, \gamma = \sqrt{1-\alpha^2-\beta^2} \tag{1.20}$$

Putting these values in equation 1.17,

$$F\,(\alpha/\lambda,\beta/\lambda;0) = \iint_{-\infty}^{\infty} E(x,y,0)\exp\left[-i2\pi\left(\frac{\alpha}{\lambda}x+\frac{\beta}{\lambda}y\right)\right]\text{dxdy} \tag{1.21}$$

Consider that $E(x,y,z)$ is the field at a distance z on the parallel plane from $E(x,y,0)$. Equation 1.21 at a distance z is given as,

$$F\,(\alpha/\lambda,\beta/\lambda;z) = \iint_{-\infty}^{\infty} E(x,y,z)\exp\left[-i2\pi\left(\frac{\alpha}{\lambda}x+\frac{\beta}{\lambda}y\right)\right]\text{dxdy} \tag{1.22}$$

Complex field E(x, y, z) can be written as,

$$E(x,y,z) = \iint_{-\infty}^{\infty} F\,(\alpha/\lambda,\beta/\lambda;z)\exp\left[i2\pi\left(\frac{\alpha}{\lambda}x+\frac{\beta}{\lambda}y\right)\right]\text{dxdy} \tag{1.23}$$

This complex amplitude must satisfy Helmholtz equation,and thus by putting the value of E(x,y,z) in the Helmholtz equation,

$$\frac{d^2}{dz^2}E\left(\frac{\alpha}{\lambda},\frac{\beta}{\lambda};z\right)+\left(\frac{2\pi}{\lambda}\right)^2\left[1-\alpha^2-\beta^2\right]F\left(\frac{\alpha}{\lambda},\frac{\beta}{\lambda};z\right)=0 \tag{1.24}$$

A solution to equation 1.24 can be given as,

$$F\left(\frac{\alpha}{\lambda},\frac{\beta}{\lambda};z\right)=F\left(\frac{\alpha}{\lambda},\frac{\beta}{\lambda};0\right)\exp\left(i\frac{2\pi}{\lambda}\sqrt{1-\alpha^2-\beta^2}z\right) \tag{1.25}$$

A relation between angular spectrum at z=0 and distance z gives knowledge about an optical field at distance z. This angular spectrum scheme provides a propagation method based on the contribution of plane wave components and their propagation in diffraction. Eq. 1.25 demonstrates that for $\alpha^2+\beta^2<1$, a change of the relative phases of the various components of the angular spectrum occurs on propagation over distance z. However, for the case when $\alpha^2+\beta^2>1$, the exponential factor in Eq. 1.25 becomes imaginary, and the wave components get attenuated on propagation. These wave components, called evanescent waves, attenuate rapidly during propagation. Finally, the optical wave field at the plane z can be written as,

$$\begin{aligned}E(x,y,z)=\iint_{-\infty}^{\infty}F\left(\frac{\alpha}{\lambda},\frac{\beta}{\lambda};0\right)\exp\left(j\frac{2\pi}{\lambda}\sqrt{1-\alpha^2-\beta^2}z\right)\\ \times\operatorname{circ}\left(\sqrt{\alpha^2+\beta^2}\right)\exp\left[j2\pi\left(\frac{\alpha}{\lambda}x+\frac{\beta}{\lambda}y\right)\right]d\frac{\alpha}{\lambda}d\frac{\beta}{\lambda}\end{aligned} \tag{1.26}$$

where the circ function restricts the range of integration to the region $\alpha^2+\beta^2<1$.

An example of how the diffraction pattern changes on propagation using an angular spectrum scheme is shown in Fig.1.9. The propagation effect on an airy pattern is examined for different propagation distances such as z=50,100,250,500,750 and 1000 mm.

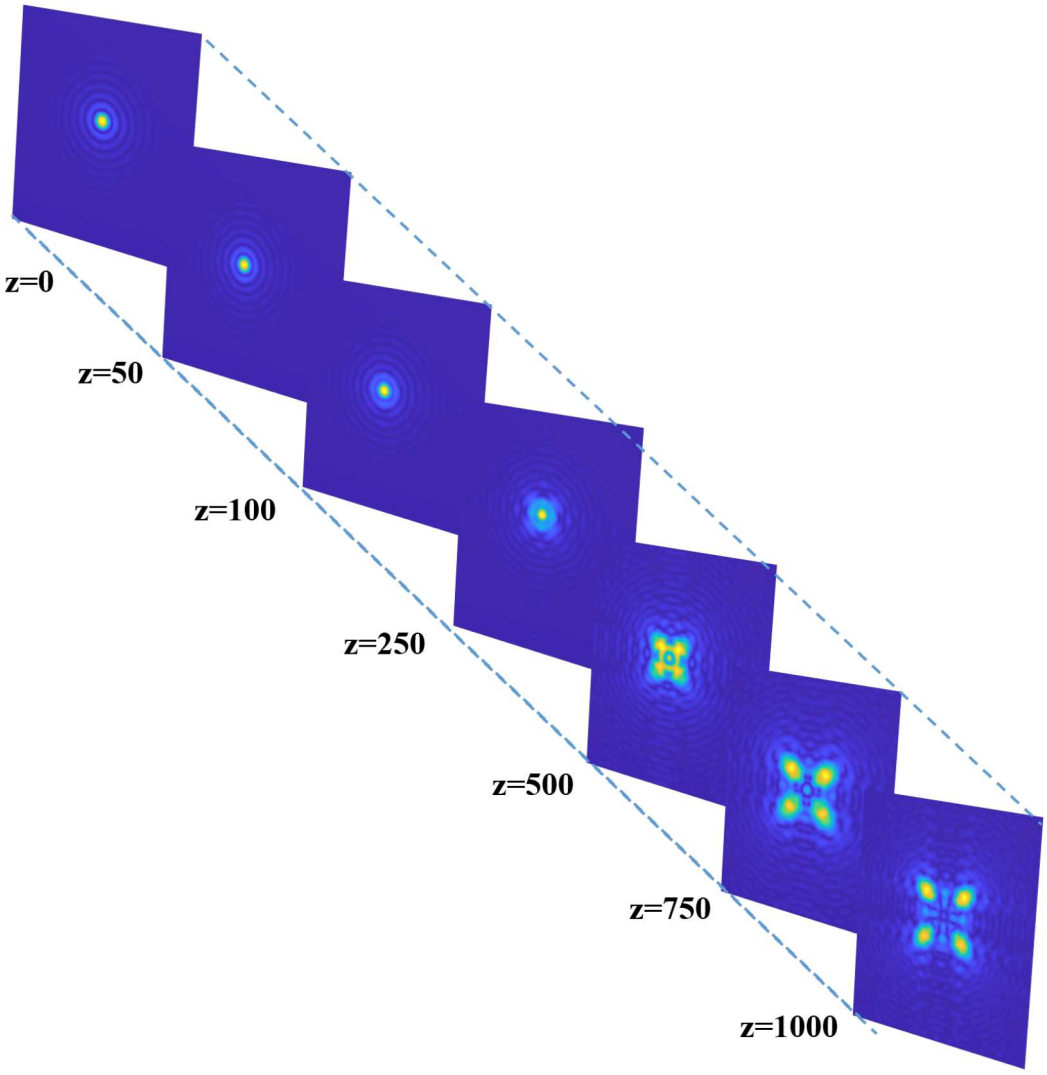

Fig. 1.9 Angular spectrum method: Effect of different propagation distances

1.4 Coherence

To study more about the statistical features of the light field, we define coherence which is a result of interference phenomenon between light vibrations at various locations in an optical field. Interference patterns provide a quantitative measure of coherence between light vibrations at different space-time points[8, 9]. For the practical point of view, we consider a quasi-monochromatic light source whose effective bandwidth is much smaller than its mean frequency, such that,

$$\frac{\Delta\omega}{\bar{\omega}} << 1 \tag{1.27}$$

In this case,consider a light field $E(r,t)$ with spatial point r and at time t,

$$E(r,t) = a(r,t)\exp(i(\phi(t) - \bar{\omega}t)) \tag{1.28}$$

where $a(r,t)$ is the amplitude at position r, and time t. $(\phi(t) - \omega t)$ represents the phase with mean frequency $\bar{\omega}$. Suppose that a quasi-monochromatic light illuminating two pinholes in Young's interference experiment, as shown in Fig. 1.10.

A superposition of two light fields $E_1(r,t)$ and $E_2(r,t)$ at point P with spatial coordinate r is given by,

$$E(r,t) = E_1(r,t-t_1) + E_2(r,t-t_2) \tag{1.29}$$

The averaged intensity distribution is represented as,

$$I(r) = \langle E^*(r,t)E(r,t)\rangle \tag{1.30}$$

$$\begin{aligned} I(r) = {} & \langle E_1^*(r,t-t_1)E_1(r,t-t_1)\rangle + \langle E_2^*(r,t-t_2)E_2(r,t-t_2)\rangle \\ & + \langle E_1^*(r,t-t_1)E_2(r,t-t_2)\rangle + \langle E_1(r,t-t_1)E_2^*(r,t-t_2)\rangle \end{aligned} \tag{1.31}$$

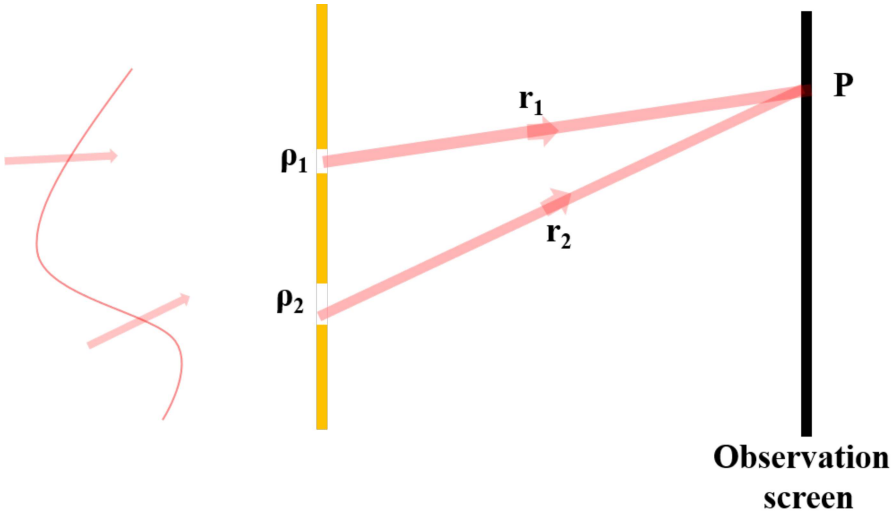

Fig. 1.10 Young's Interference Experiment

Equation 1.31 can be re-written as,

$$I(r) = I_1(r) + I_2(r) + 2Re\langle E_2^*(r,t-t_2)E_2(r,t-t_2)\rangle + 2Re[\langle E_1^*(r,t-t_1)E_2(r,t-t_2)\rangle] \tag{1.32}$$

where *Re* represents the real part. Finally, making use of Eq. 1.30, averaged intensity can be written as,

$$I(r) = I_1(r) + I_2(r) + 2Re[\sqrt{I_1(r)}\sqrt{I_2(r)}\gamma(\rho_1,\rho_2,\tau)] \tag{1.33}$$

where $\tau = t_1 - t_2$ and γ is the *complex degree of coherence* which evidently measures the statistical similarity of light fields at point ρ_1 and ρ_2 (points at source plane). γ can be represented in terms of mutual coherence function $W(\rho_1,\rho_2,\tau)$

$$\gamma(\rho_1,\rho_2,\tau) = \frac{W((\rho_1,\rho_2,\tau))}{\sqrt{I_1(r)I_2(r)}} \tag{1.34}$$

where $W(\rho_1,\rho_2,\tau) = \langle E^*(\rho_1,t)E(\rho_2,t+\tau)\rangle$ is also known as cross-correlation function. Over more simplification, the complex degree of coherence may be represented by the

following,

$$I(r) = I_1(r) + I_2(r) + 2\sqrt{I_1(r)}\sqrt{I_2(r)}|\gamma(\rho_1,\rho_2,\tau)|\cos\left[\alpha(\rho_1,\rho_2,\tau) - \delta\right] \tag{1.35}$$

where $\delta = \bar{\omega}\tau$. Eq. 1.35 represents the interference law for stationary optical fields. For a special case,when $I_2(r)$ =$I_1(r)$, Eq. 1.35 becomes,

$$I(r) = 2I_1(r)[1 + |\gamma(\rho_1,\rho_2,\tau)|\cos[\alpha(\rho_1,\rho_2,\tau) - \delta]] \tag{1.36}$$

The maximum and minimum average intensity is given by,

$$I_{max}(r) = 2I_1(r)[1 + |\gamma(\rho_1,\rho_2,\tau)|] \tag{1.37}$$

$$I_{max}(r) = 2I_1(r)[1 - |\gamma(\rho_1,\rho_2,\tau)|] \tag{1.38}$$

The visibility of fringes $V(r)$ provides a measure of coherence function, where $V(r)$ is given by,

$$V(r) = \frac{I_{max}(r) - I_{min}(r)}{I_{max}(r) + I_{min}(r)} \tag{1.39}$$

Using Eq. 1.37 and 1.38 in Eq. 1.39, Eq. 1.39 becomes,

$$V(r) = |\gamma(\rho_1,\rho_2,\tau)| \tag{1.40}$$

Eq. 1.40 relates the modulus of the complex degree of coherence to a readily measurable quantity (visibility). $|\gamma| = 1$ is the case of complete coherence. On the other hand, a fully incoherent light source has $|\gamma| = 0$. A condition when $0 < |\gamma| < 1$ represents the partial coherent source. Complex degree of coherence $\gamma(\rho_1,\rho_2,\tau)$ offers a quantitative description of spatial and temporal coherence. The ability of a light beam to interfere with the delayed version of itself to form fringes controls temporal coherence. On the other hand, spatial

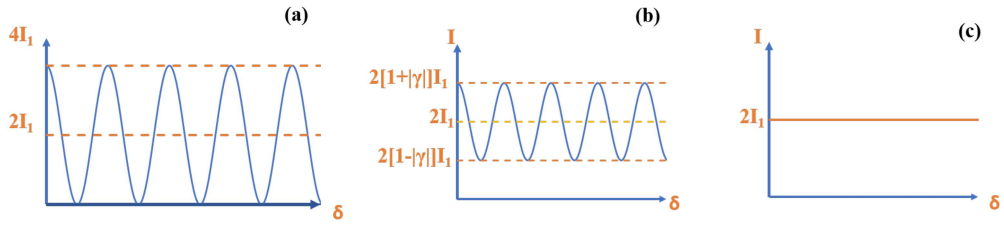

Fig. 1.11 The distribution of average intensity for different degrees of coherence cases

coherence is defined by the ability of light to interfere with a spatially shifted version of itself. It is represented by $\langle E_1^* E_2 \rangle$ and provides the correlation of light field between two spatially separated points, without any time delay between them. Fig. 1.11 represents the distribution of average intensity for different values of degree of coherence when $I_2(r)$ =$I_1(r)$. Fig. 1.11(a) is the case of coherent superposition, i.e., $\gamma = 1$. Fig. 1.11(b) and (c) represent the partially coherent and incoherent condition, i.e., $0 < |\gamma| < 1$ and $\gamma = 0$, respectively.

1.5 Holography

Holography is a robust technique that permits to retain amplitude as well as phase information of the light field. This scheme records the interference pattern of the light field emanating from the light source, which encodes both its amplitude and phase information in its fringe pattern. The interference pattern recorded in holography is then reconstructed either optically or digitally to read/obtain the recorded light field. Digital recording of the hologram and its numerical reconstruction, known as digital holography(DH), has revolutionized holography. The availability of high-quality detectors with large numbers of pixels and advanced computational facilities have enormously contributed to the exponential growth of DH. Moreover, digital reconstruction of the hologram has led to the quantitative reconstruction of the light field(rather than qualitative), and this approach has led to the

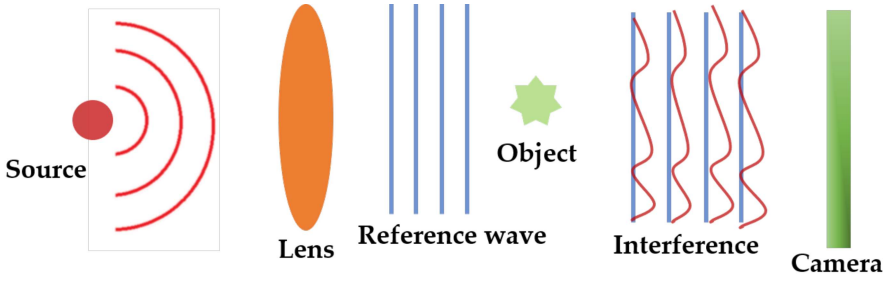

Fig. 1.12 Schematic of an inline holography geometry

development of quantitative label-free imaging techniques. In order to cover some of the basic principles of holography, we briefly cover some of the major geometries with historical aspects. In this section, our main focus is to introduce the concept of holography with the interference of coherent waves.

Consider an interference of coherent waves coming from an object $E(r)$ and reference $R(r)$ at the observation plane. Total intensity as a result of interference of both waves is given as,

$$I(r) = |E(r)+R(r)|^2 = E(r)E^*(r)+R(r)R^*(r)+E(r)R^*(r)+R(r)E^*(r) \tag{1.41}$$

where asterisk $*$ represents the complex conjugate and $I(r)$ is the hologram with r being the spatial coordinate at observation plane. The first two terms are the unmodulated terms, also called dc terms. The last two terms are responsible for phase reconstruction in digital holography.

Gabor, in 1948, discovered that utilizing the coherent reference wave along with the scattered wave diffracted by the object can provide amplitude and phase information of the scattered wave. This type of scheme used for the three-dimensional(3D) reconstruction of objects is termed inline holography. A schematic is shown in Fig. 1.12. However, in inline holography, the dc term and last two terms are overlapped in the reconstruction since there is no separation among the reference and objects beams. This is known as a twin

image issue and imposes difficulties in retrieving desired object information. An angular separation of the reference beam in off-axis holography is required to overcome the twin image problem of in-line holography.

1.5.1 Off-axis holography

The presence of twin image issues in inline holography was tackled by Leith and Upatnieks by developing an off-axis reference wave to the object wave at some tilt/angle, as shown in Fig. 1.13. This circumvents the twin image of inline holography by reconstructing

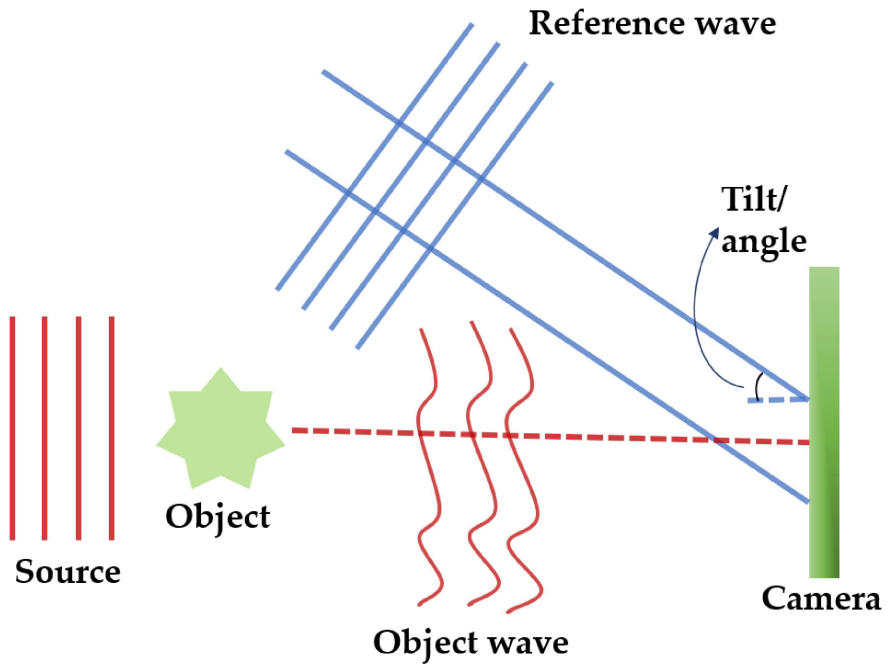

Fig. 1.13 Conceptual design for holographic recording in an Off-axis holography scheme

separate copies of the object and its complex conjugate. Off-axis holography needs a carrier frequency to record the hologram in order to prevent the conjugate image from overlapping with the reconstructed image. However, the field of view (FOV) is restricted as a result of the limited sizes of available detectors and frequency space sharing [10].

1.5.2 Phase shifting Digital Holography

To enhance the limited FOV in the off-axis, phase-shifting holography [11, 12, 13] was proposed, which takes multiple images and accurately changes the phase between each successive image. Yamaguchi et al. proposed a phase-shifting DH [13] by providing multiple phase shifts in the reference wave to determine the amplitude and phase of the sample. A schematic of phase-shifting digital holography is shown in Fig. 1.14. The phase shifts can be provided by using a piezoelectric transducer [13], a liquid crystal phase modulator [14], spatial light modulators(SLMs) etc. In addition to these advancements,

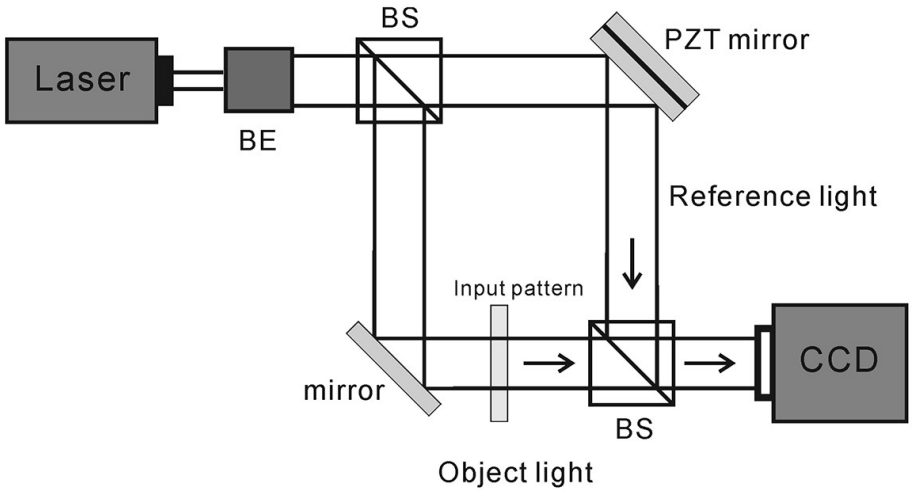

Fig. 1.14 Phase Shifting Digital Holography [15]

common path holographic designs have been developed by various researchers, which are relatively compact and stable [16, 17, 18]. A detailed discussion of such common path schemes is given in chapter 2. Moreover, in recent years, DH has been explored and extended to the polarization regime, and the scheme is called Polarization digital holography(PDH). Details are discussed in the next section.

1.6 Polarization digital holography

The idea to employ DH as a polarization imaging technique was first put forth by Lohmann [19]. Many works for polarization measurement approaches then queued up. Complete information of the optical field of the object is obtained with additional information of polarization with amplitude and phase.

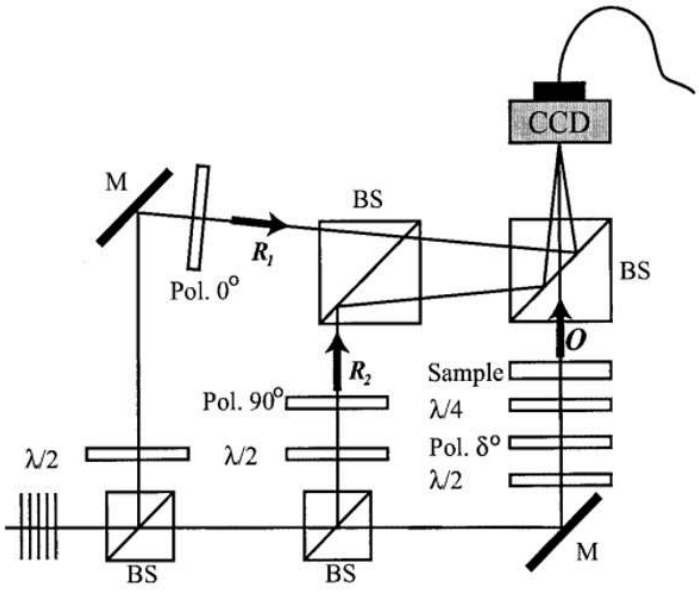

Fig. 1.15 Polarization Imaging Interferometer [20]

The interference pattern for orthogonal electric field components is represented as,

$$I_x(x,y) = |E_x(x,y) + R(x,y)|^2 \tag{1.42}$$

$$I_y(x,y) = |E_y(x,y) + R(x,y)|^2 \tag{1.43}$$

where I_x and I_y are the interference patterns corresponding to two orthogonal components.E_x and E_y are the two orthogonal electic field components of the sample. $R(x,y)$ represents

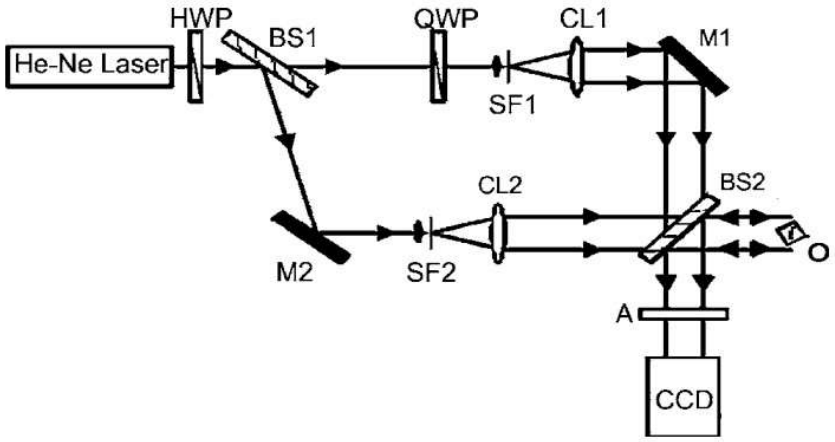

Fig. 1.16 On-axis Polarization Imaging Scheme [12]

the reference wave. Colomb et al. [20] used coherent beam interference to define the polarization state of a sample. This method creates holograms by interfering with the object beam with two orthogonally polarised reference beams. Intensity and phase are obtained by numerically reconstructing the wavefront for both polarisation states. As shown in Fig 1.15, a half-wave plate and a polarizer are employed to regulate the wave's intensity and polarization state in both reference arms, R1 and R2. The polarization of the beam illuminating the object can be modified with the polarizer and the quarter wave plate. An off-axis geometry is used to record the hologram, with each wave traveling in its own path.

An on-axis polarization holography scheme was proposed by Nomura et al. [12], which uses specific phase shifts between the two orthogonal reference waves, as shown in Fig. 1.16. Another polarization scheme was developed by Tahara et al. [21] for single-shot imaging. In this technique, single-shot imaging was achieved through the use of simultaneous phase-shifting interferometry and space division multiplexing techniques, as shown in Fig. 1.17. After going through a phase array, the reference has a spatially periodic distribution. A micro polarizer array is used to image the periodic phase distribution onto

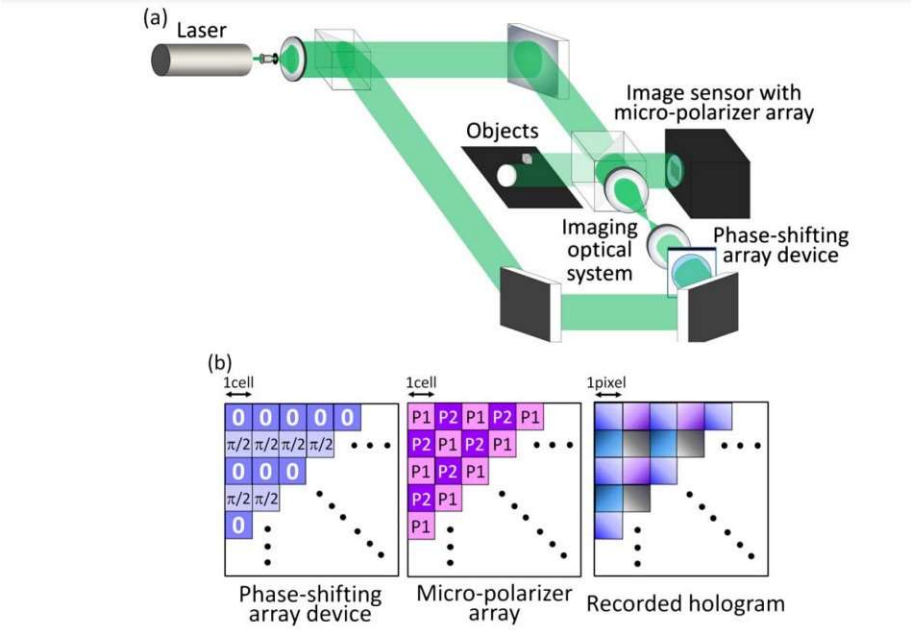

Fig. 1.17 Single shot polarization Imaging Interferometer [21]

the image plane, selecting information from various polarizations cell by cell. In another work by Naik et al., the accurate polarimetric measurement is proposed without using any prior knowledge of the reference beam and the spatial carrier frequency. This is accomplished using an integrated calibration scheme which reduces the influence of the errors in the reference field and the spatial carrier frequency as in conventional polarimetric schemes. An experimental design for this scheme is given in Fig. 1.18. Moreover, the Jones matrix imaging technique has been used to use polarization digital holography to study light-matter interactions of coherent light [23].

A common path digital holographic schemes have played a significant role where noise and vibrations are an issue. These methods utilize a compact and common path for object and reference beams and thus create a stable experimental setup. A few common path experimental designs are proposed and discussed in Ref. [16, 17, 18] One such experimental geometry for the polarimetric reconstruction of an object is discussed in detail in chapter two.

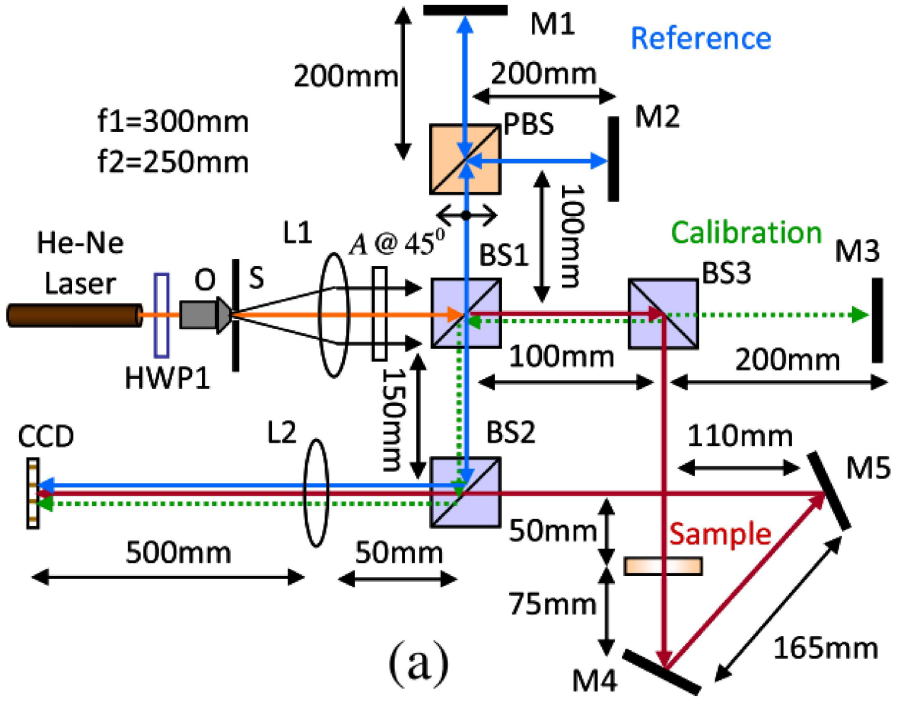

Fig. 1.18 Experimental design for interferometric polarimeter with an integrated calibration scheme [22]

1.7 Optics with randomness

1.7.1 Propagation of coherent light through randomness: Laser Speckle

A granular pattern is formed at the observation screen when coherent light is either reflected from a rough surface or propagates through a medium with random refractive index fluctuations[24]. This grainy structure is called a speckle as shown in Fig. 1.19. Speckles are formed due to the interference of the coherent waves scattered by optically rough patterns in the propagation path [24, 25]. Speckles are also formed when laser light is transmitted through stationary diffusers because the optical paths of different light rays passing through the object vary significantly. Due to the height variations of the rough surface, the phases of the waves scattered by various surface sites change statistically. Speckle formed by the interaction of coherent light with a rough surface is shown in Fig.

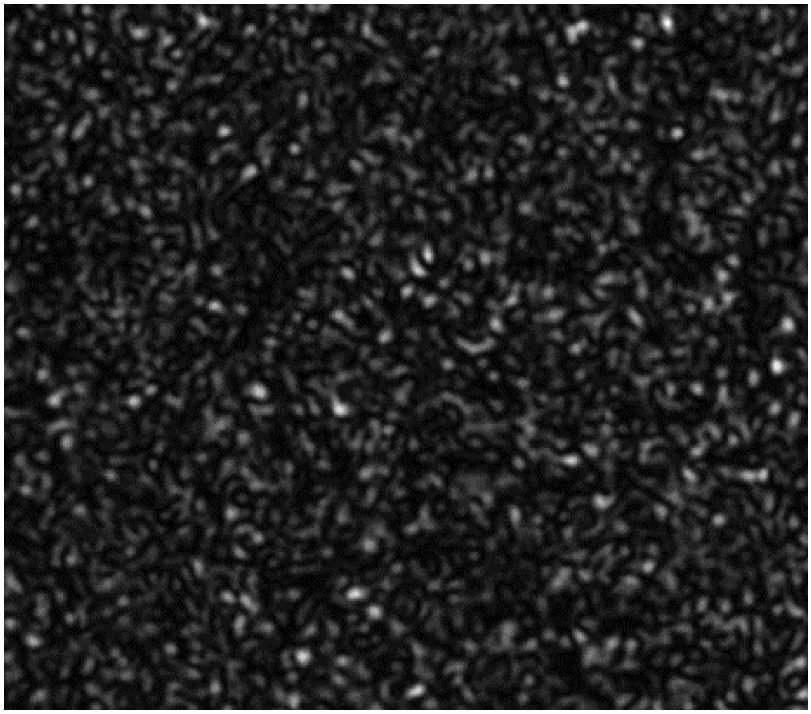

Fig. 1.19 Laser Speckle

1.20. Generally, both the coherence of the incident light and the specific characteristics of the random surface or media affect the statistical properties of the speckle patterns. Randomness is found in nature, in atmospheric turbulence, fog, etc. Propagation of waves through such randomness is a challenging yet very practical problem in various fields, such as imaging in atmospheric turbulence, looking through fog, rain, and biomedical imaging, etc. These speckles do not provide any direct information about the incident light. However, the scattered waves carry a signature of the incident wave, and the information is retrieved using numerous techniques. A few approaches have been developed to counteract this scattering effect, such as phase conjugation, transmission matrix, adaptive optics method, and so on. Other than these, an essential tool is correlation optics which plays a vital role in retrieving information whenever the light is being scattered from a random media. The mentioned schemes are discussed briefly below.

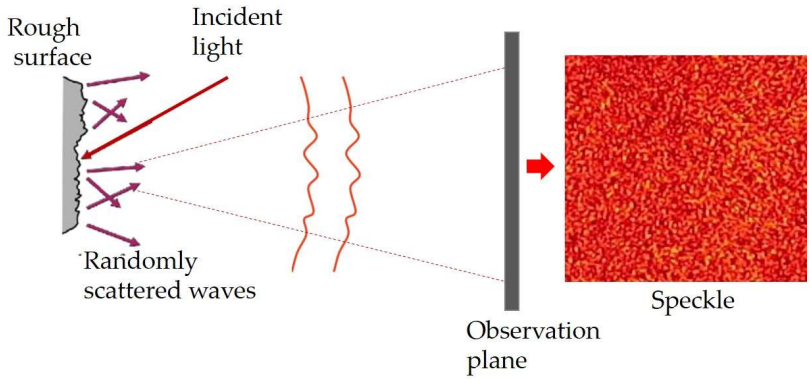

Fig. 1.20 A speckle formed by the interaction of coherent light with rough surface

1.7.2 Adaptive optics

The goal of adaptive optics is to identify and correct distorted wavefronts caused by random or inhomogeneous media. The principle behind adaptive optics is to detect the distorted wavefront using a wavefront sensor and then use a deformable mirror or other optical element to correct the wavefront in real time. This is usually done by using phase conjugation techniques. These schemes involve the reversal of the incoming wave phase and the compensation of wavefront distortion. This is achieved through a closed-loop system that iteratively feeds back information from a wavefront sensor to a control computer, which in turn drives a deformable mirror to correct the wavefront of the light continuously. A typical adaptive approach scheme is shown in Fig. 1.21, designed for the case of atmospheric turbulence. Initially intended for telescopes, adaptive optics is a method now used in various applications, such as confocal microscopy and two-photon microscopy, to improve the imaging quality [26]. Adaptive optics methods have provided a solution for imaging through non-homogeneous media. However, they are still subject to certain limitations, such as the weight of the adaptive mirror, the complexity and cost of the systems, the requirement of specialized hardware such as deformable mirrors, wavefront sensors, control systems, no. of modes required to correct the highly distorted wavefronts, etc.

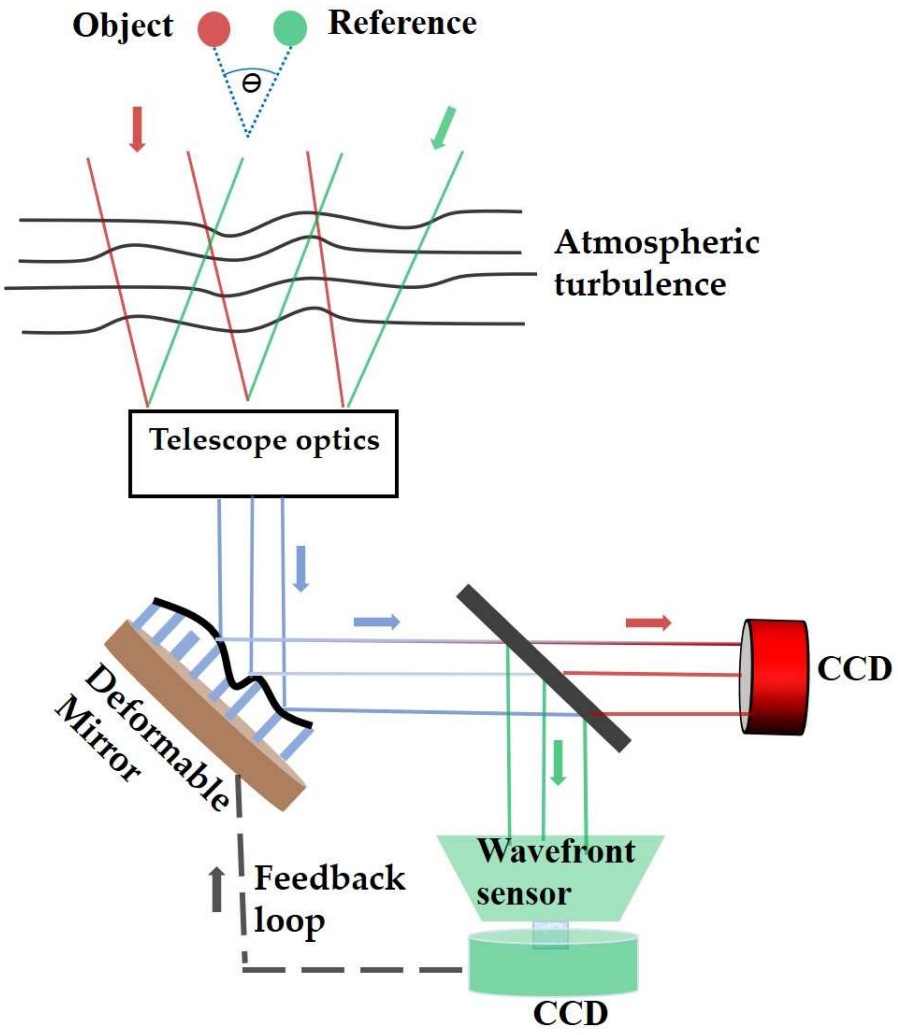

Fig. 1.21 A schematic of adaptive optics approach

1.7.3 Optical phase conjugation

Optical phase conjugation (OPC) can reconstruct the real, distorted wavefront necessary for phase distortion compensation to match the original wavefront (as depicted in Fig. 1.22). OPC allows the scattered light to be phase conjugated (also known as time-reversed)

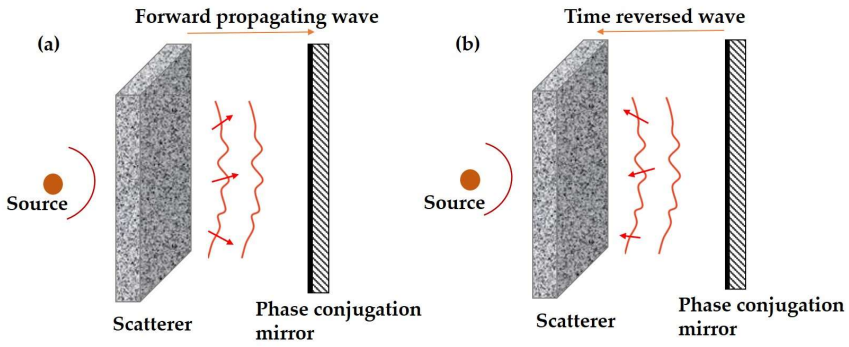

Fig. 1.22 Optical phase conjugation scheme

back to the scattering medium, causing scattered photons moving along various optical paths to interfere constructively at the targeted position. Fig. 1.22(a) represents the forward propagating wave, and Fig. 1.22(b) shows the corresponding time-reversed wave. Nonlinear crystals have been used to generate optical phase conjugation effect [28]. Few applications lie in retrieving two-dimensional image information through scattering media using the OPC [27]. An experimental scheme for the same is given in Fig. 1.23, where a stable and robust Sagnac-like ring-type interferometer is used for the digital phase conjugation approach. Moreover, phase conjugation has been described using digital holography that combines a dynamic computer-generated holography technique with a spatial light modulator (SLM) [29].

1.7.4 Schemes based on Transmission matrix(TM)

The use of transmission matrix to tackle random media has been explored by many researchers. By monitoring the scattering media's TM and utilizing the deterministic linear

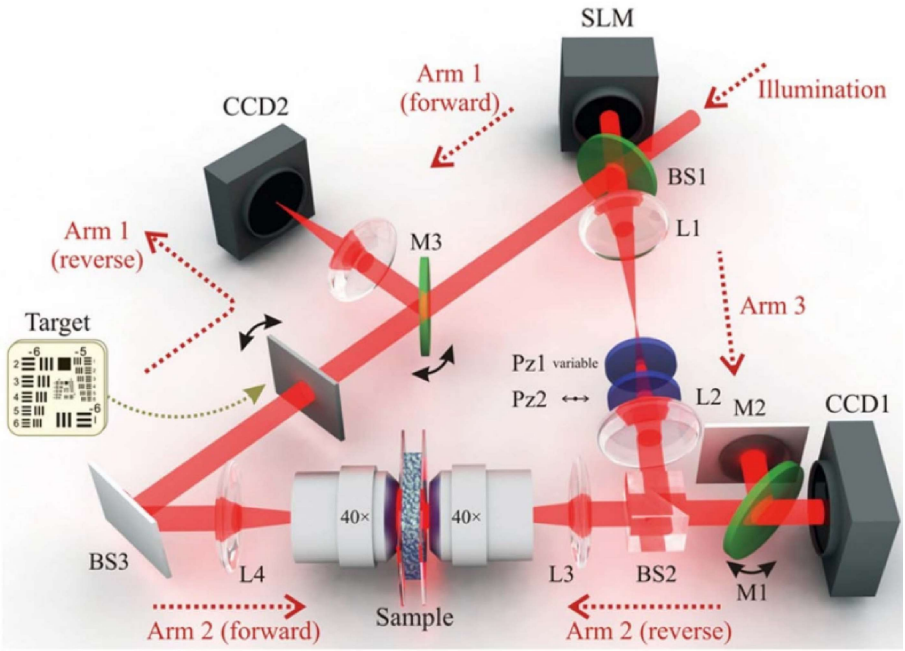

Fig. 1.23 Optical schematic for a ring-interferometer digital optical phase conjugation [27]

relationship between the TM and the image distortion, the image distortions caused by the scattering medium can be canceled to a large extent and light can be focused as desired. Popoff et al. first proposed a scheme to experimentally measure the transmission matrix of the complex medium in optics for monochromatic light[30]. A design to record the transmission matrix with spatial light modulator(SLM) is shown in Fig. 1.24. The optical field in the m^{th} output-free mode and the one in the n^{th} input-free mode are connected by the complex coefficients k_{mn} in the TM for a given wavelength. Thus, the projection E_n^{out} of the outgoing optical field on the m^{th} free mode is given by $E_n^{out} = \sum_n k_{mn} E_n^{in}$ where E_n^{in} is the complex amplitude of the optical field in the n^{th} incoming free mode. In another attempt, the idea of programmable spectrum shaping is introduced to focus the polychromatic light through randomness and also make a desired spectrum. This scheme is known as programmable spectrum filtering and is shown in Fig. 1.25. The modulation effect generated by the SLM is wavelength-dependent.To find a suitable phase map for modifying the wavefront of the polychromatic light, a feedback-based system is developed

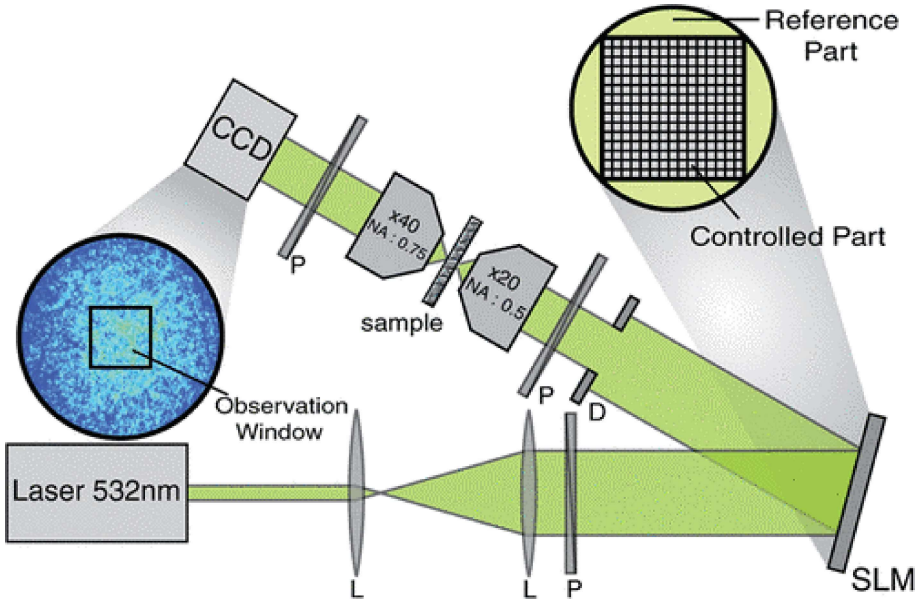

Fig. 1.24 A schematic to record transmission matrix [30]

that iterates in accordance with the correlation coefficient. This causes the filtered target to produce the desired spectral shape. Above mentioned techniques work on the principle of cancellation of randomness. However, the majority of the techniques are sensitive to the alignment and wavelengths of the incident light. On the other hand, new trends are also emerging where the randomness of the light is used rather than cancellation for different reasons. Among these techniques, the correlation property of random light is one of the highly explored areas of research, and some of these methods are briefly touched on here in accordance with the main objectives of this thesis.

1.7.5 Correlation optics

Correlation optics has evolved into an exceptionally fascinating and promising domain in modern optics with diverse technological developments ranging from imaging to communication, from astronomy to industrial metrology, etc. Recent development and the

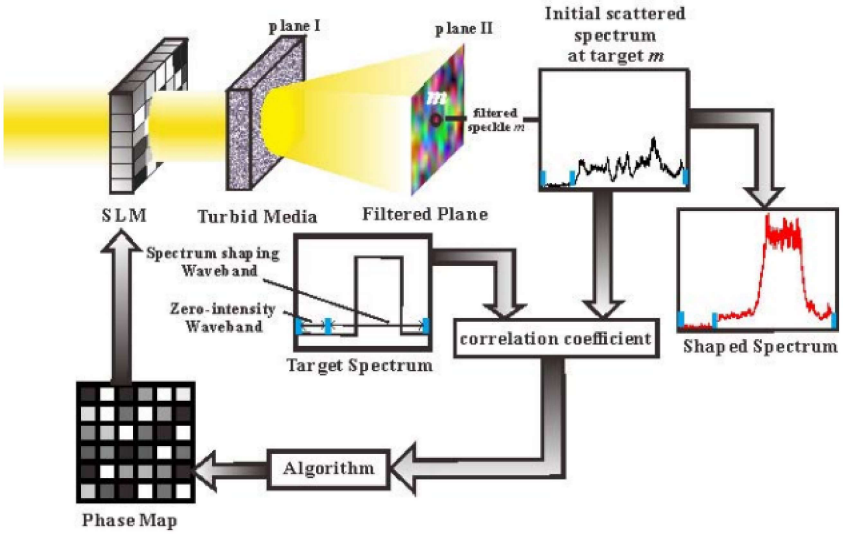

Fig. 1.25 A schematic of programmable spectrum shaping [31]

introduction of new illumination sources have inspired researchers to utilize the random light and correlation principle for advanced imaging.

Optical Memory Effect

A novel class of optical imaging schemes has been introduced by the idea of using correlations between the speckle patterns. Seminal work by Issac Freund in the early 90's on the speckle memory played a significant role in designing the scattering medium as a lens [32, 33]. The angular memory effect states that when two objects are angularly separated by a small separation, they produce identical speckle images at the observation plane except for a lateral shift in two speckle patterns.As shown in Fig. 1.26, a lateral shift in the speckle patterns at the observational plane is directly related to an angular shift in the incident beam. As a result, this scheme can be thought of as a lensless imaging system, and within the observational memory range, the distorting medium itself serves as a static lens [32, 33]. Various imaging techniques have been explored through the use of

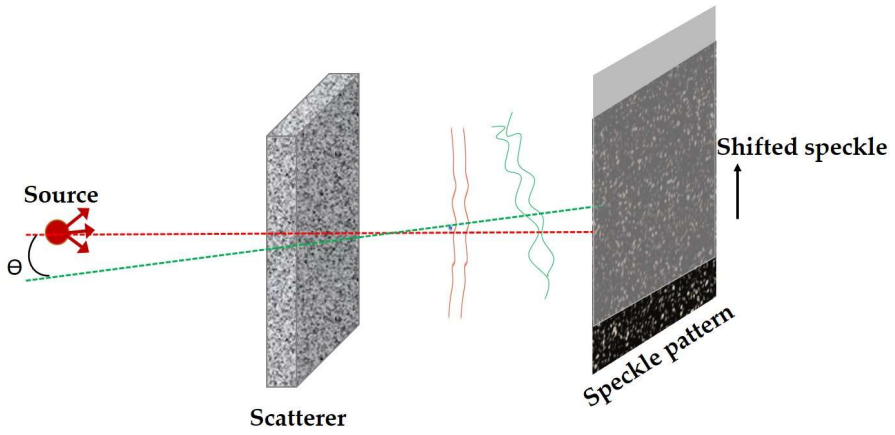

Fig. 1.26 A conceptual design for angular memory effect principle

the memory effect principle to develop imaging techniques through the scattering media [34, 35]. By combining the memory effect with the autocorrelation of intensity, Katz et al. [35, 36] developed techniques to reconstruct the image of an object from random light. These techniques employ phase retrieval to extract information from the randomness by analyzing the autocorrelation of the intensity speckle pattern [34, 36, 37].

Second order correlation function

The Michelson stellar interferometer first solved the issue of calculating the angular diameter of stars, but it suffered from extreme sensitivity brought on by outside influences. Robert Hanbury Brown and Richard Twiss developed an intensity interferometer (HBT interferometer) in 1956 that worked on the principle of correlations of intensities rather than field correlations. This brought a significant development in the characterization of light fields. The second-order interferometer was lacking some distinct and unknown properties that were revealed by the intensity correlations of the light field. The HBT interferometer scheme was initially created to gauge star sizes by examining the correlation of intensity fluctuations later used in various fields, including nuclear science, quantum optics, optical imaging, etc. These intensity correlation interferometers are less complex

and unaffected to instability brought on by outside disturbances than the interferometers with second-order field correlation. A schematic is shown in Fig. 1.27. The instantaneous

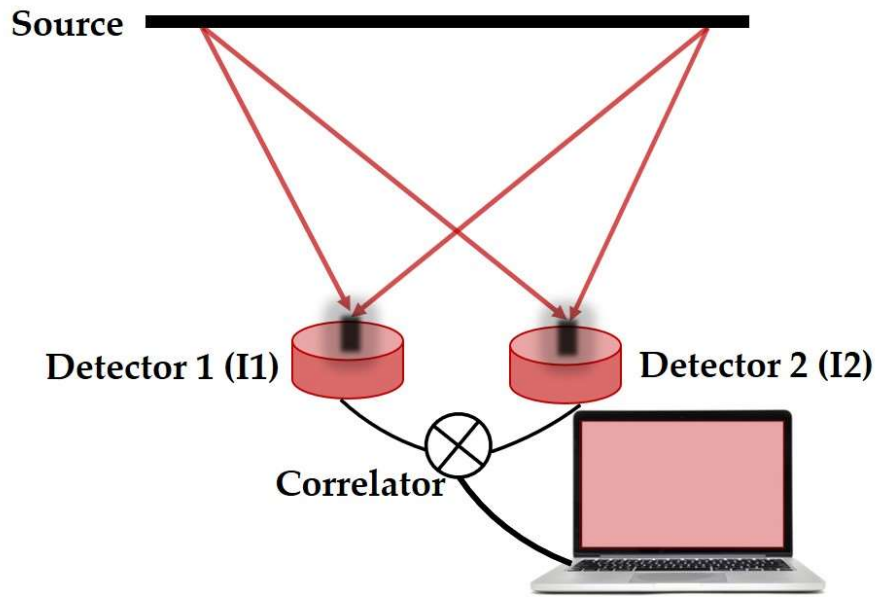

Fig. 1.27 A conceptual design for intensity correlation measurement

intensity at the observation plane is measured as,

$$I(r_j,t) = E\left(r_j,t\right) E^*\left(r_j,t\right) \tag{1.44}$$

For the monochromatic light, time 't' is ignored. $E(r_j,t)$ represents the instantaneous field at any point in space and r_j denotes the spatial position, with j=1,2. A second-order correlation function (field correlation) is represented as $g^1(r_1,r_2)$ and is given as,

$$g^1(r_1,r_2) = \langle E\left(r_1\right) E^*\left(r_2\right)\rangle \tag{1.45}$$

whereas a fourth order correlation is represented as $g^2(r_1,r_2)$ and is given as,

$$g^2(r_1,r_2) = \langle E\left(r_1\right) E^*\left(r_1\right) E\left(r_2\right) E^*\left(r_2\right)\rangle \tag{1.46}$$

Using Eq. 1.44 in 1.46,and omitting t for convenience(for a monochromatic light), intensity correlation can be mathematically expressed as,

$$g^2(r_1, r_2) = \langle I(r_1) I(r_2) \rangle \tag{1.47}$$

The intensity fluctuation at the observation plane is given by,

$$\Delta I(r) = I(r) - \langle I(r) \rangle \tag{1.48}$$

where $\langle I(r) \rangle$ represents the mean of intensity fluctuations at the observation plane. The fourth order correlation i.e., intensity correlation can be expressed in terms of second order correlation for the Gaussian random field as,

$$\langle I(r_1) I(r_2) \rangle = \langle I(r_1) \rangle \langle I(r_2) \rangle + |\langle E(r_1) E^*(r_2) \rangle|^2 \tag{1.49}$$

$$\langle \Delta I(r_1) \Delta I(r_2) \rangle = |\langle E(r_1) E^*(r_2) \rangle|^2 \tag{1.50}$$

Here parenthesis $< .. >$ represents ensemble average, and this can be realized by replacing it with either time average $< .. >_T$ or space average $< .. >_S$ or a combination of both $< .. >_{TS}$ according to the experimental conditions of stationarity and ergodicity. The relation in second and fourth-order correlation is written as,

$$g^2(r_1, r_2) = \langle I(r_1) \rangle \langle I(r_2) \rangle + |g^1(r_1, r_2)| \tag{1.51}$$

Techniques utilizing intensity correlation have made a significant contribution in several fields. Photon correlation holography is an interesting experimental method where the reconstruction of 3D objects encoded in hologram is possible using intensity correlations. [38]. However, the technique is not capable of recovering the phase due to phase loss

issue in the intensity correlation. Various techniques have been explored for retrieving phase information along with intensity. This phase loss issue can be tackled with schemes using the interference of coherence waves [39]. This technique recovers complex valued objects through the scattering media from a single speckle measurement by utilizing interference of coherence waves in the intensity correlation of the random light pattern. A schematic for the interference of two coherence waves is shown in Fig. 1.28 [39]. Here two coherence waves, one arising due to the object and the other arising due to the

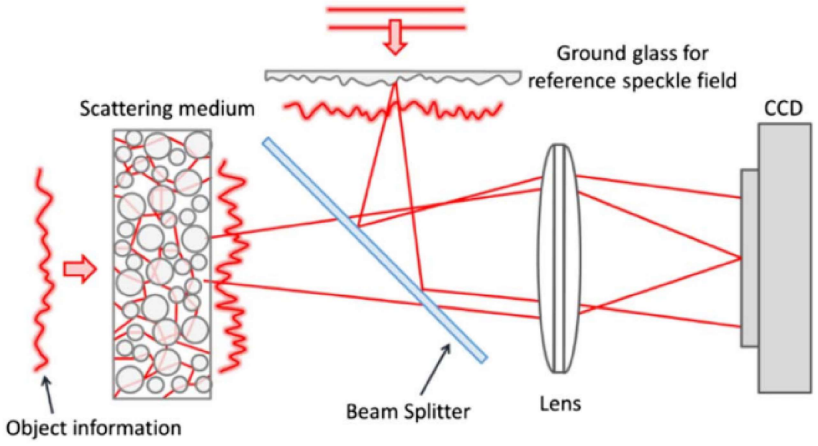

Fig. 1.28 A schematic for the interference of coherence waves [39]

reference source, interfere and make a hologram in a two-point intensity correlation. This coherence hologram is similar to the conventional hologram based on the interference of optical fields. A lensless Fourier transform coherence holography technique was also demonstrated by Singh et al., where the spatial stationarity is achieved at the observation plane even in the Fresnel domain due to interference of two independent random fields and intensity correlation of this spatially fluctuating random field is expressed in lensless Fourier transform hologram [40].

1.7.6 Polarization Speckle

Along with intensity fluctuations, fluctuations in spatial polarization may take place when coherent light propagates through an anisotropic random medium, and such coherent field is referred to as polarization speckle [41, 42]. A schematic for the generation of polarization speckles is shown in Fig. 1.29.

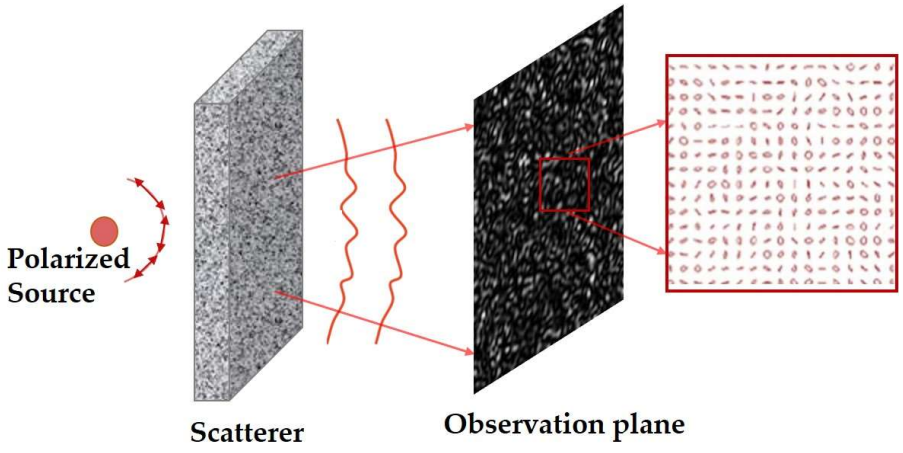

Fig. 1.29 A conceptual design for the generation of polarization speckle

A Poincare sphere or polarization ellipse representation can be used to represent the state of polarization(SoP) of a light field. An example is shown in Fig. 1.29 and 1.30 for the SoP of a random polarized field. To express polarization mathematically in the case of coherent waves, four instantaneous Stokes parameters (SPs) can be used to explain the polarization state of a coherent light field at a single point as given below,

$$S_0(r) = E_x(r)E_x^*(r) + E_y(r)E_y^*(r) \tag{1.52}$$

$$S_1(r) = E_x(r)E_x^*(r) - E_y(r)E_y^*(r) \tag{1.53}$$

$$S_2(r) = E_x(r)E_y^*(r) + E_y(r)E_x^*(r) \tag{1.54}$$

$$S_3(r) = i(E_x(r)E_y^*(r) - E_y(r)E_x^*(r)) \tag{1.55}$$

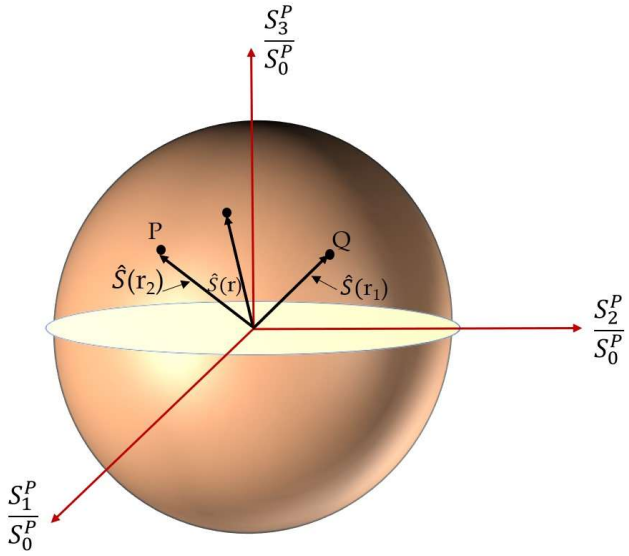

Fig. 1.30 Poincare sphere representing Stokes vectors

The polarization and coherence, when studied combinedly, provided significant theories to characterize the statistical light fields. A unified theory of coherence and polarization can be understood in detail from [9]. A 2×2 matrix known as a coherence polarization(CP) matrix is used to represent the statistical properties of the random polarized field, given by the following,

$$W(r_1,r_2)=\begin{bmatrix} <E_x(r_1)E_x^*(r_2)> & <E_x(r_1)E_y^*(r_2)> \\ <E_y(r_1)E_x^*(r_2)> & <E_y(r_1)E_y^*(r_2)> \end{bmatrix}=\begin{bmatrix} W_{xx}(r_1,r_2) & W_{xy}(r_1,r_2) \\ W_{yx}(r_1,r_2) & W_{yy}(r_1,r_2) \end{bmatrix} \tag{1.56}$$

Elements of the coherence polarization (CP) matrix may take complex values as they represent a two-point correlation of the light field for orthogonal basis $i,j=x,y$.

For a single point, equation 1.56 transforms to a polarization matrix defined as,

$$W(r,r)=\begin{bmatrix} W_{xx}(r,r) & W_{xy}(r,r) \\ W_{yx}(r,r) & W_{yy}(r,r) \end{bmatrix} \tag{1.57}$$

where $W_{ij}(r,r)$=$\langle E_i(r)E_j^*(r)\rangle$ represents the correlation of orthogonal field components at the same point. Elements of this polarization matrix can also be used to define the averaged Stokes parameters as follows,

$$\langle S_0(r)\rangle = W_{xx}(r,r) + W_{yy}(r,r) \tag{1.58}$$

$$\langle S_1(r)\rangle = W_{xx}(r,r) - W_{yy}(r,r) \tag{1.59}$$

$$\langle S_2(r)\rangle = W_{xy}(r,r) + W_{yx}(r,r) \tag{1.60}$$

$$\langle S_3(r)\rangle = i(W_{xy}(r,r) - W_{yx}(r,r)) \tag{1.61}$$

Recently attempts have also been made to extend and apply the intensity correlation approach to the vector light field and such extension has offered new insights into the physical optics and applications. Moreover, attempts to unify the coherence and polarization in a single framework have steered new trends in coherence optics, particularly in dealing with light with non-uniform polarization structures. Elements of the CP matrix are complex, and they follow wave equations similar to the optical field [9]. Using this feature, interference of the elements of the CP matrix can be used to develop some unconventional holography techniques through randomness. The characterization has been used to develop new phase-shifting holography techniques such as phase-shifting with the HBT approach which relies on equation,

$$(W_{xy}(\Delta r) + W_{xy}^{\phi}(\Delta r))^2 \tag{1.62}$$

where $W_{xy}^{\phi}(\Delta r)$ represents the phase-shifted coherence wave and the technique is used to recover unknown $W_{xy}(\Delta r)$ from the intensity correlation. An experimental geometry is shown in Fig. 1.31. Moreover, these off-diagonal elements of the CP matrix have also been used to extend the field of view in the correlation holography [43].

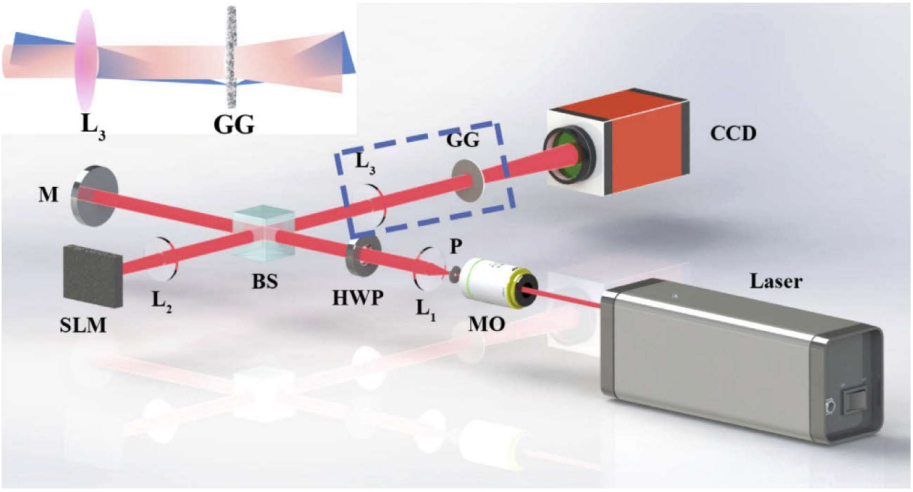

Fig. 1.31 Experimental setup for phase imaging of target behind scattering medium with phase shifting [44]

Few studies have been initiated to use intensity correlation for vector fields in the space-time domain, and it has been highlighted that intensity correlation can be used to analyze the electromagnetic degree of coherence [45]. For the field adhering the Gaussian statistics, a relation is found between the electromagnetic degree of coherence and intensity correlation in terms of contributions from all four elements of the coherence-polarization matrix. Setala et al. [46] extended the study to the space-frequency domain and proposed that the spectral level of electromagnetic coherence affects the spectral HBT effect. It has also been demonstrated that the degree of cross-polarization affects the correlation of intensity fluctuations between two detectors [47, 48]. The two-point intensity correlation in the same cross-section of a random electromagnetic beam can be examined in terms of source parameters [49]. A significant contribution has been made by Singh et al. Our group has also significantly contributed to the coherence optics, particularly on the synthesis and application of the random light in the imaging [50, 51, 52]. Considering the Gaussian random process, the correlation of the cross-covariance at two points is given as,

$$\langle \Delta I(r_1)\Delta I(r_2)\rangle = \sum_{i,j}(|W_{ij}(r_1,r_2)|^2 \tag{1.63}$$

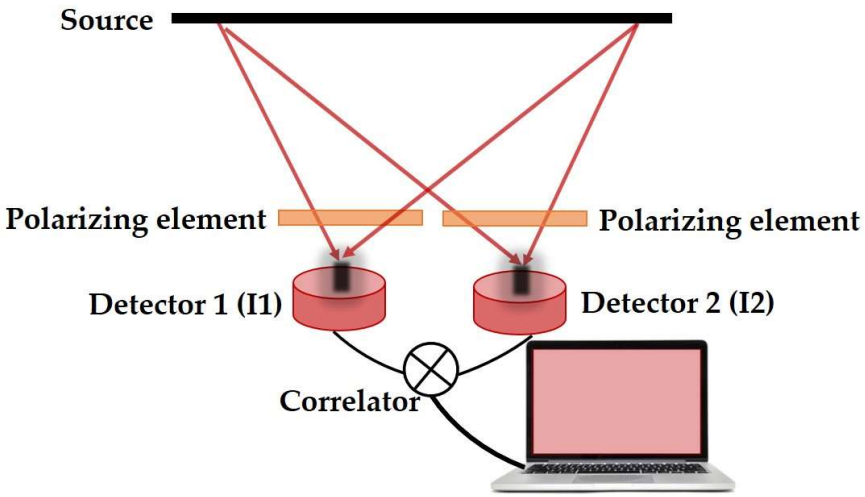

Fig. 1.32 A conceptual design for intensity correlation measurement of vector field

A schematic of the propagation of the random polarized light field and its analysis by two intensity detectors is shown in Fig. 1.32. Two polarizing elements are used before two detectors for measuring the CP matrix elements. Besides the intensity correlations, the correlation of the Stokes parameters at two points can also be used to characterize the random vector fields.

A schematic to experimentally measure the Stokes parameters is shown in Fig. 1.33. Two polarizing elements, a quarter-wave plate and a polarizer, are placed before two detectors to measure the polarization states of the light field. A theoretical background to evaluate correlations in these Stokes fluctuations is given below. Fluctuations in the SPs are represented as [5, 53],

$$\Delta S_n(r) = S_n(r) - \langle S_n(r) \rangle \tag{1.64}$$

Where n=0,1,2,3 and S_n represent the four Stokes parameters at the observation plane. $\langle S_n(r) \rangle$ represents the mean, i.e., ensemble-averaged quantity. A correlation between these Stokes fluctuations corresponding to different Stokes parameters provides information about the polarization of the incident light field. A two-point correlation can be expressed

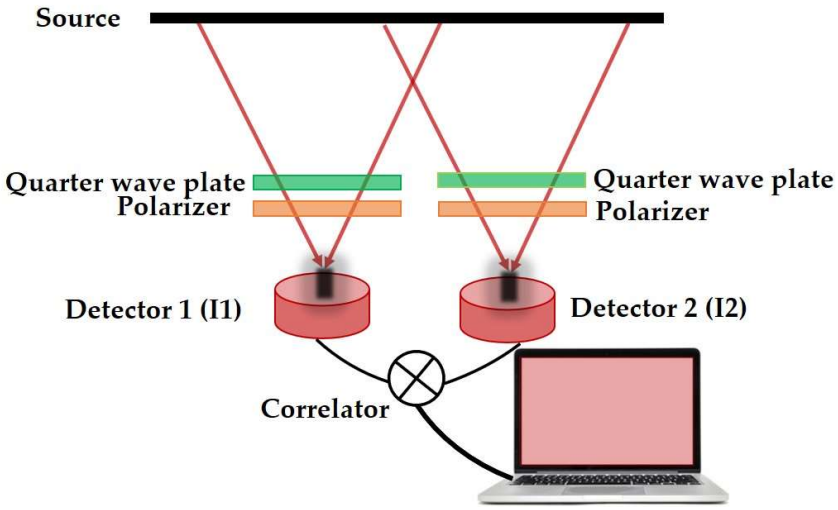

Fig. 1.33 A conceptual design for the measurement of Stokes parameters correlation

as,

$$C_{nm}(r_1, r_2) = \langle \Delta S_n(r_1) \Delta S_m(r_2) \rangle \tag{1.65}$$

A specific relation of the correlation of these stokes fluctuations, i.e., $C_{nm}(r_1, r_2)$, has been used for an application in polarimetry in the last chapter of the thesis.

These correlation techniques can be used to analyze the speckle pattern and are found to be useful in various fields such as astronomy, imaging, sensing, etc. Correlation-based techniques make use of speckle patterns rather than canceling them as used in adaptive optics, wavefront shaping, and phase conjugation schemes. This makes the correlation-based schemes a significant tool for providing more accurate and simple imaging methods.

The next chapters of this thesis focus on randomness, i.e., speckle pattern. Thus, it is necessary to understand how this randomness is used in various research areas. Randomness acts as a hurdle in a few techniques, as mentioned above, such as adaptive optics, wavefront shaping, phase conjugation schemes, etc. However, schemes based on correlation make use of this speckle for various imaging applications and do not consider speckle or randomness an obstacle. A schematic of dividing these techniques into two parts is shown in Fig. 1.34. Some examples where a random field is present by

compulsion are atmospheric turbulence, scattering walls, looking through random media, etc. Schemes have been developed to find the depth of the object behind the scattering medium [36, 54]. Another category is where a random field is used by choice; for example, a speckle field illumination-based holography, correlation holography with a single-pixel detector, ghost imaging, ghost diffraction, etc. A chart of how randomness can be utilized in different ways is given below. Basically, we have divided the randomness into two main categories one, where randomness is canceled (I), and another, where randomness is utilized for different imaging and microscopic schemes(II). Work done in this thesis make use of randomness and provides significant information from it rather than canceling the randomness. Moreover, the work described in the thesis lies in the category (II, B) of Fig. 1.34. Ghost imaging and ghost diffraction, which is a correlation-based imaging method, is also realized with the use of two static random patterns. Details are discussed in the next chapters of the thesis.

In conclusion, this chapter covers different aspects of light with arbitrary coherence. The discussion started with a coherent light and its diffraction. A detailed theoretical basis is covered to explain the propagation of coherent light, and later this is extended to coherence and polarization of light.

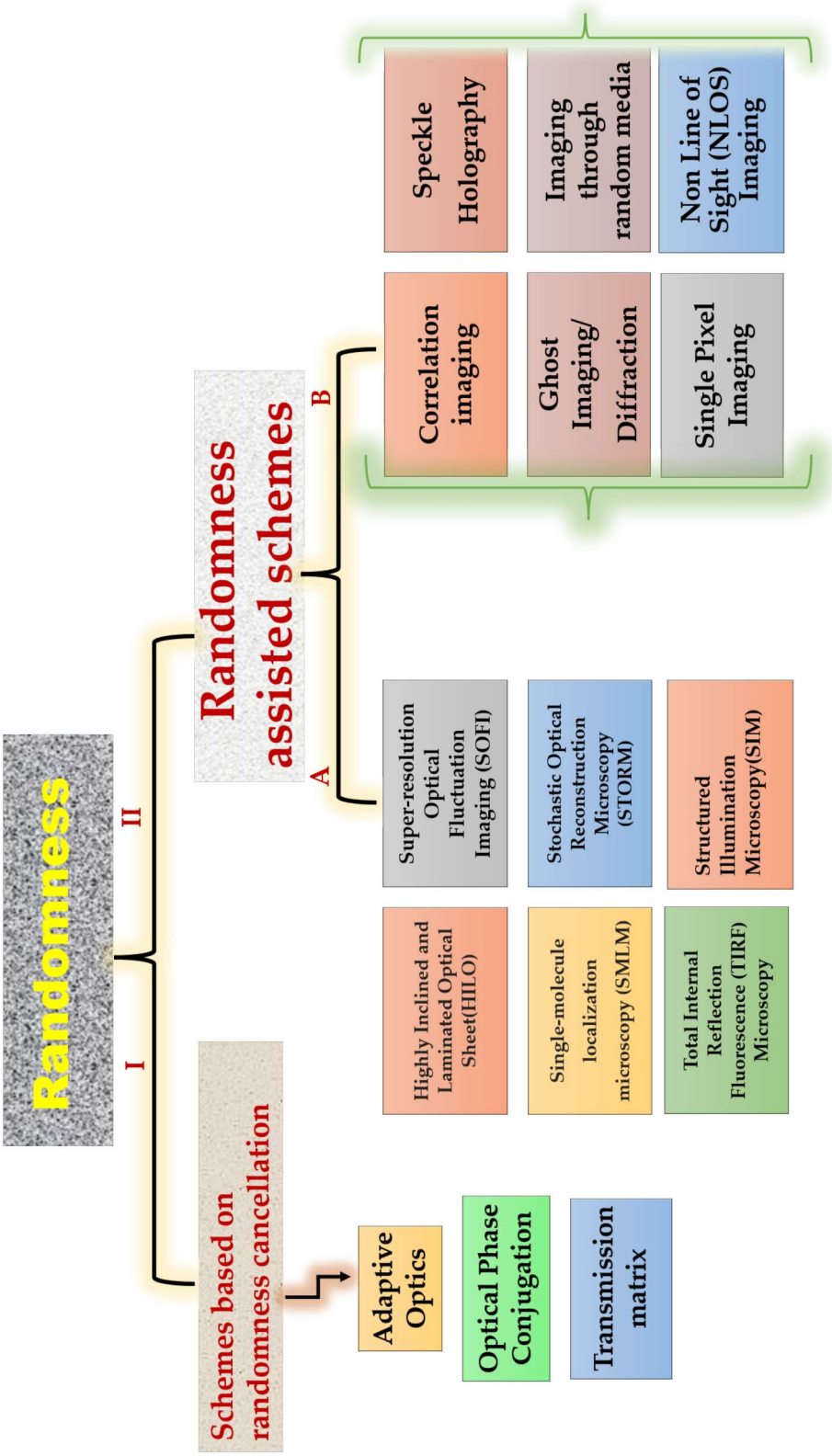

Fig. 1.34 Application of randomness in different research areas